New Journal of Physics
The open access journal at the forefront of physics
Deutsche Physikalische Gesellschaft DPG IOP Institute of Physics

PAPER • OPEN ACCESS

Enhanced laser-driven hadron sources with nanostructured double-layer targets

To cite this article: L Fedeli *et al* 2020 *New J. Phys.* **22** 033045

New Journal of Physics
The open access journal at the forefront of physics

Deutsche Physikalische Gesellschaft DPG
IOP Institute of Physics

Published in partnership with: Deutsche Physikalische Gesellschaft and the Institute of Physics

CrossMark

OPEN ACCESS

RECEIVED
20 September 2019

REVISED
24 January 2020

ACCEPTED FOR PUBLICATION
10 February 2020

PUBLISHED
24 March 2020

PAPER

Enhanced laser-driven hadron sources with nanostructured double-layer targets

L Fedeli[1,2], A Formenti[1], A Pazzaglia[1], F M Arioli[1,3], A Tentori[1,4] and M Passoni[1]

[1] Department of Energy, Politecnico di Milano, Italy
[2] presently at LIDYL, CEA-Saclay, France
[3] presently at CEA/DES/IRESNE/DEC, Cadarache, France
[4] presently at Université Bordeaux 1, France

E-mail: arianna.formenti@polimi.it

Keywords: laser-driven ion acceleration, ultra-intense lasers, neutron sources, nanostructured targets, particle-in-cell simulations, Monte Carlo simulations

Abstract

Laser-driven ion sources are approaching the requirements for several applications in materials and nuclear science. Relying on compact, table-top, femtosecond laser systems is pivotal to enable most of these applications. However, the moderate intensity of these systems ($I \lesssim 10^{19}$ W cm^{-2}) could lead to insufficient energy and total charge of the accelerated ions. The use of solid foils coated with a nanostructured near-critical layer is emerging as a promising targeted solution to enhance the energy and the total charge of the accelerated ions. For an appropriate theoretical understanding of this acceleration scheme, a realistic description of the nanostructure is essential, also to precisely assess its role in the physical processes at play. Here, by means of 3D particle-in-cell simulations, we investigate ion acceleration in this scenario, assessing the role of different realistic nanostructure morphologies, such as fractal-like foams and nanowire forests. With respect to a simple flat foil, the presence of a nanostructure allows for up to a $\times$ 3 increase of the maximum ion energy and for a significant increase of the conversion efficiency of laser energy into ion kinetic energy. Simulations show also that the details of the nanostructure morphology affect both the maximum energy of the ions and their angular distribution. Furthermore, combined 3D particle-in-cell and Monte Carlo simulations show that if accelerated ions are used for neutron generation with a beryllium converter, double-layer nanostructured targets allow to greatly enhance the neutron yield. These results suggest that nanostructured double-layer targets could be an essential component to enable applications of hadron sources driven by compact, table-top lasers.

1. Introduction

Ion acceleration driven by ultra-intense laser pulses is a well established reasearch topic [1–3]. In state-of-the-art Petawatt-class laser facilities, few nanocoulomb, relatively collimated, broad spectrum ion bunches can be accelerated up to a ~100 MeV [4–6] cut-off energy. Target normal sheath acceleration (TNSA) [7] is arguably the most robust and widely studied ion acceleration scheme. In TNSA an ultra-intense laser pulse interacts with a thin solid foil, heating the electrons of the target up to several MeV energies. The expanding electron cloud generates an intense electric field at the back side of the target. This electric field is then responsible for the ion acceleration process. Historically, the foreseen societal application in radiotherapy [8, 9] has been a preeminent driving force behind research efforts on laser-driven ion acceleration. However, existing laser-driven ion sources still fall short of the stringent requirements in terms of energy, monochromaticity and stability [10]. Indeed, up to now, laser-driven ion sources have been routinely used only as a diagnostic tool for transient electromagnetic fields in laser-plasma interaction experiments [11–13].

Especially in recent years, materials and nuclear science have emerged as a promising domain of application of laser-driven ion sources. Proof-of-principle experiments [14] and numerical works [15–17] support the feasibility of laser-driven ion beam analysis for non-destructive materials characterization. Laser-driven ion sources have been considered to test electronic components in a harsh radiation environment [18], for thermal stress testing [19], to study ultra-fast dynamics in irradiated materials [20, 21], and for materials synthesis [22, 23]. Ultrashort pulsed neutron sources driven by laser-accelerated ions [24–32] have been investigated for applications such as fast neutron spectroscopy [33] and radiography [34].

What make these applications particularly attractive are the requirements for the ion source. Energies of few MeVs are perfectly suitable for several ion beam analysis techniques [35] or to generate neutrons with a lithium [36] or beryllium [37] converter. Moreover, for selected applications, the inherently broad energy spectrum of a laser-driven ion source [2] is not detrimental [15, 17] and could even be beneficial [18]. Maximum ion energies of ~1 MeV have been recently demonstrated even with commercial, sub-terawatt laser systems [38]. These laser-systems are truly table-top and can operate at a high repetition rate (kiloHertz). Relying on these systems could make laser-driven ion sources portable and competitive with conventional accelerators, paving the way for their widespread adoption in materials and nuclear science.

Over the years, several advanced ion acceleration schemes have been proposed to enhance the properties (maximum energy, angular distribution, total charge …) of the accelerated ions [2, 39, 40], which could be very beneficial for several of the aforementioned applications. In some scenarios where the ion energy is a critical issue, the use of advanced ion acceleration strategies could even enable a particular application on a given laser system. Neutron conversion is emblematic of this last case, since it is crucial to reach at least the energy threshold for the nuclear reaction.

Among the advanced ion acceleration schemes, the use of foils coated with a low-density, near-critical, nanostructured layer [41, 42] as a target for TNSA is emerging as a promising strategy [43–51]. Here, 'near-critical' means having an electron density close to the critical one, $n_c = \pi m_e c^2/\lambda^2 e^2$ (where m_e is the electron mass, λ is the laser wavelength and e is the elementary charge). n_c marks the density threshold for electromagnetic wave transparency. Ultra-intense laser interaction with a plasma having a near-critical density is characterized by a strong coupling and an efficient energy absorption [52–54]. The low-density layer can either be a controlled pre-plasma or a solid nanostructured material with ultra-high void fraction. Both solutions allow for a high absorption efficiency of the laser energy by the hot electrons population, which results into more ions accelerated at higher energies with respect to a simple flat foil [55–57]. Nevertheless, pre-plasmas—usually generated via target pre-expansion induced by the laser pedestal or ns-duration pulses [58, 59]—is affected by poor stability and control, since large deviations may arise depending on the specific laser facility. Indeed, within the literature on laser-driven ion acceleration, the pre-expansion of the target was reported to lead to very different results: ranging from strong enhancement [60], to mild enhancement [57] or even a reduction [61] of the effectiveness of the acceleration process. Conversely, a nanostructured low-density layer can be produced with tunable and finely controlled properties, which, combined with an in-depth characterization, should lead to more reproducible experimental conditions. For a given envisaged application of laser-driven ion sources, the enhancement due to the advanced targetry would allow to dramatically reduce the requirements on the laser driver. Cheaper, more compact and higher repetition rate lasers could be used for applications which otherwise would have required more powerful, more expensive and definitely non-portable systems.

An accurate theoretical understanding of laser-driven ion sources based on double-layer targets (DLTs) is essential to guide experimental investigations and ultimately to enable applications of these sources. However, the presence of a nanostructured layer poses considerable modeling challenges. Indeed,the exceptional temporal contrast of modern day laser facilities [62–64] could allow a nanostructure to survive long enough to affect the interaction. In previous numerical works [65, 66], we observed that a detailed modeling of the nanostructure morphology is crucial for a reliable description of the physical processes at play.

In this work, by means of fully 3D particle-in-cell simulations, we model an experimental scenario of enhanced laser-driven ion acceleration where the target is a solid foil coated with a low-density nanostructured layer. A realistic morphology is used for the nanostructured layer and the laser parameters are those of a typical 30–50 Terawatt-class system. We consider two realistic morphologies for the low-density nanostructured coating (a fractal-like foam and a forest). We also couple the results of our particle-in-cell simulations to Geant4 [67] Monte Carlo (MC) code, in order to simulate the conversion of laser-accelerated ions into neutrons [68, 69], which is a promising application of laser driven ion acceleration. DLTs having a uniform near-critical layer with the same average density of the nanostructured layers are considered as well for comparison. Figure 1 illustrates the general setup and the numerical framework adopted in this work.

Our simulations show that the presence of a nanostructure allows for a significant increase of the maximum ion energy and of the total number of accelerated ions, with the details of the nanostructure morphology affecting both the maximum energy and the angular distribution of the accelerated ions. This translates directly into more neutrons being emitted per laser shot.

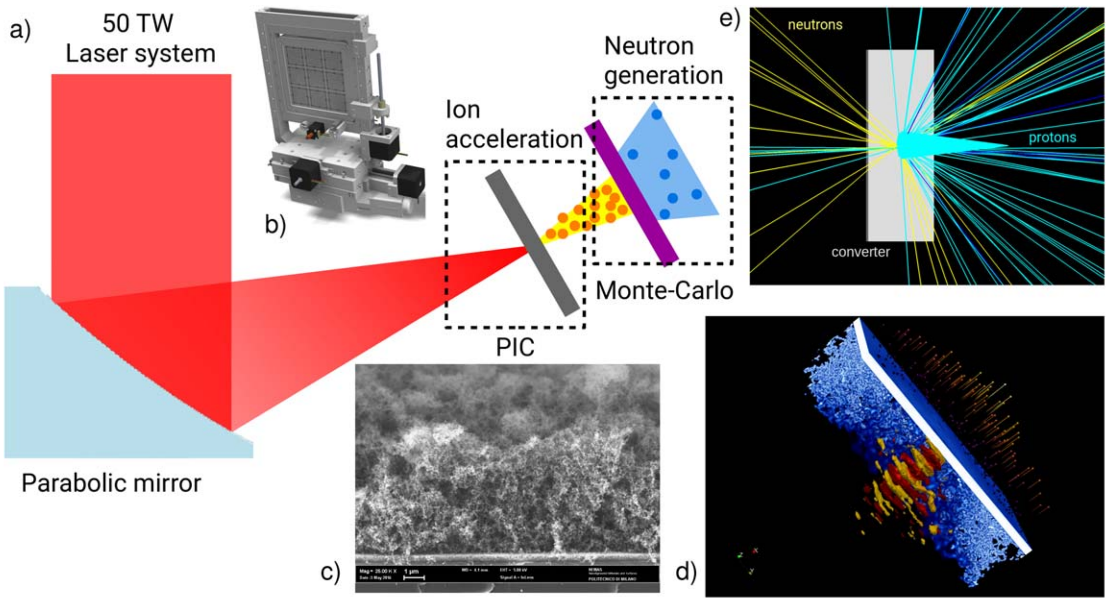

Figure 1. Scheme of the numerical framework adopted for this work. (a) Typical parameters of a 50 TW table-top laser system are considered (b) The use of targetry solutions for repetitive operation is considered to estimate total yields over several minutes. (c) Scanning electron microscope picture of a nanostructured low-density foam similar to those used in [48, 49]. (d) 3D particle-in-cell simulations are used to model laser-driven ion acceleration (reproduced with permission from [70]). (e) Laser-accelerated ions are fed into the Geant4 Monte Carlo code to simulate neutron generation in a beryllium converter.

2. Methods

Our work is based on two numerical tools: particle-in-cell and MC simulations. This section describes in detail the methods and codes used in this work and the parameters of the simulations. In the following we will consider a laser wavelength $\lambda = 800$ nm, as for a Ti:sapphire laser system.

2.1. Particle-in-cell simulations

Particle-in-cell simulations are a standard numerical technique to investigate laser-plasma interaction [71, 72]. For our 3D simulations we relied on the open source, massively parallel *piccante* code [73]. The numerical box was $100\lambda \times 60\lambda \times 60\lambda$, with periodic boundary conditions. The spatial resolution was 40 points per λ (ppλ) in each direction, while the temporal resolution was 98% of the Courant condition. The total duration was 80 λ/c. The laser beam had a Gaussian spatial profile with a waist equal to 5 λ and a $\cos^2$ temporal profile with a FWHM for the fields equal to 15 λ. These parameters model an idealized, high contrast, Ti:sapphire laser system with tens of TW power. The beam was linearly polarized and the angle of incidence was 0°. The normalized intensity was $a_0 = 4$ ($a_0 = eA/m_e c^2$, where e is the elementary charge, A is the vector potential, m_e is the electron mass and c is the speed of light).

Concerning the target, ions were initialized perfectly cold, while electrons were initialized with a very small temperature (few eV). The substrate—i.e. the flat solid foil or bare target—was 0.5 λ thick, with an electron density of 40 n_c. We decided to use an electron density of only 40n_c for the substrate because 3D simulations with a more realistic density for a highly ionized target (∼100 n_c) would have required a huge computational effort. However, we performed convergence tests with 2D simulations to assess the appropriateness of our choice for both the solid foil density and the resolution. We let the density of the solid foil vary among 20 n_c, 40 n_c and 80 n_c, while the resolution varies between 40 ppλ and 60 ppλ. The main results of these 2D tests are shown in figure 2, where the protons spectra at time 80λ/c are shown for (a) a simple 0.5 λ-thick solid foil and (b) a DLT modeled with a uniform near-critical layer with 2.14 n_c density and 4 λ thickness. Increasing the electron density of the substrate from 20 n_c to 80 n_c did not result in any appreciable change of the ion energy spectrum for the DLT. Instead, a strong reduction of the maximum ion energy was observed for the simple flat target under the same density variation. Nonetheless, when doubling the density from 40 n_c to 80 n_c only a slight reduction is obtained. These results confirm that using a substrate density of 40 n_c in our simulations should not significantly affect the results presented in this manuscript. Overall, a solid density of 40 n_c is found to be a good compromise: large-enough to be overdense, but low-enough to let us resolve the skin depth of the laser with a resolution of 40 ppλ. In any case, to ascertain the goodness of such a resolution value, we also tested a higher resolution of 60 points per λ in 2D geometry and we observed negligible differences in the proton spectra (see figure 2).

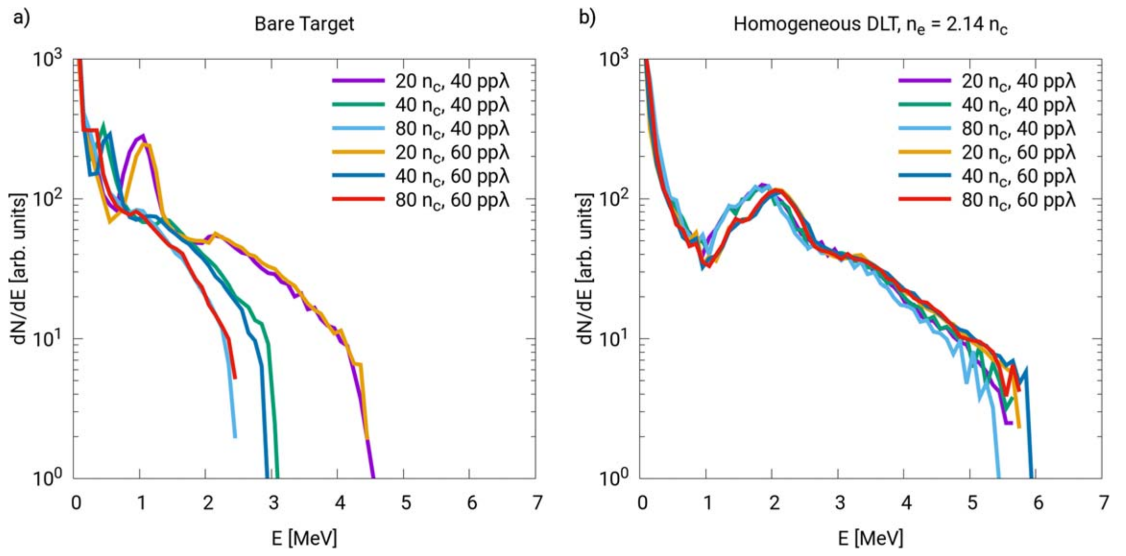

Figure 2. Proton spectra at time 80 λ/c obtained in the 2D PIC convergence tests varying the resolution (40 and 60 points per λ) and the density of the solid foil (20 n_c, 40 n_c and 80 n_c) for (a) the bare target case and (b) a double-layer target with a homogeneous near-critical layer of 2.14 n_c density and 4 λ thickness.

Table 1. Comparison between homogeneous and nanostructured near-critical layers used in the 3D PIC simulations.

	Near-critical layers	
Morphology	Homogeneous	Foam-like and random wires
Filling factor	100%	3.8% and 5.7%
Local electron density	1.5 n_c and 2.29 n_c	40 n_c
Average electron density	1.5 n_c and 2.29 n_c	1.5 n_c and 2.29 n_c
Thickness	4 λ	4 λ

40 macro-electrons per cell and 2 macro-ions with $Z/A = 0.5$ per cell were used. The hydrocarbon contaminant layer was 0.05 λ thick with an electron density of 7 n_c, a proton density of 1 n_c and a fully ionized carbon density of 6 n_c (64 macro-particles per cell per species were used). The low-density layer was chosen to be 4 λ thick. Three different morphologies (an idealized uniform plasma, a fractal-like nanostructured foam and a random nanowires forest) and two different average densities (1.5 n_c and 2.29 n_c) were considered as well as the case of a simple flat target for comparison, for a total of seven simulations. Both the realistic morphologies considered here are representative of low-density nanostructured materials used in laser-plasma interaction experiments [48, 49, 74, 75].

The foam layer is generated through an extension of the diffusion-limited cluster-cluster aggregation model (DLCCA), designed to simulate the structure of fractal aggregates, such as colloids and soot [76] (a detailed description of the method is provided in [66]). The building blocks of the fractal aggregates are nanospheres having a local electron density of $\sim$40 n_c, arranged in such a way that the filling factor is 5.7% and 3.8% for the two density values. The radii of the nanospheres are 0.05λ for the higher density foam and 0.047 λ for the lower density foam. Nanowires forests are modeled as a collection of cylinders, with a radius of 0.12 λ and an inclination angle extracted randomly from a uniform distribution between -30° and $+30^\circ$ with respect to laser axis. The nanowires have a local electron density of $\sim$40 n_c and their number is chosen so that the filling factor is either 5.7% or 3.8%. For the nanostructured layers 40 macro-electrons per cell and 2 macro-ions with $Z/A = 0.5$ per cell were used, while for the uniform layers 4 macro-electrons per cell and 1 macro-ion with $Z/A = 0.5$ per cell were used. The main properties of the near-critical layers are summarized in table 1. All the considered near-critical layers are coupled to a substrate with 0.5 λ thickness and 40 n_c electron density.

We point out that the nanostructures show large local fluctuations of their average density on scales comparable with the laser waist (5λ). Figures 3(a) and (b) show the density profiles of the near-critical layers integrated over a transverse region of size 25λ^2 and 100λ^2, respectively. On the illuminated region (size $\sim$100λ^2,

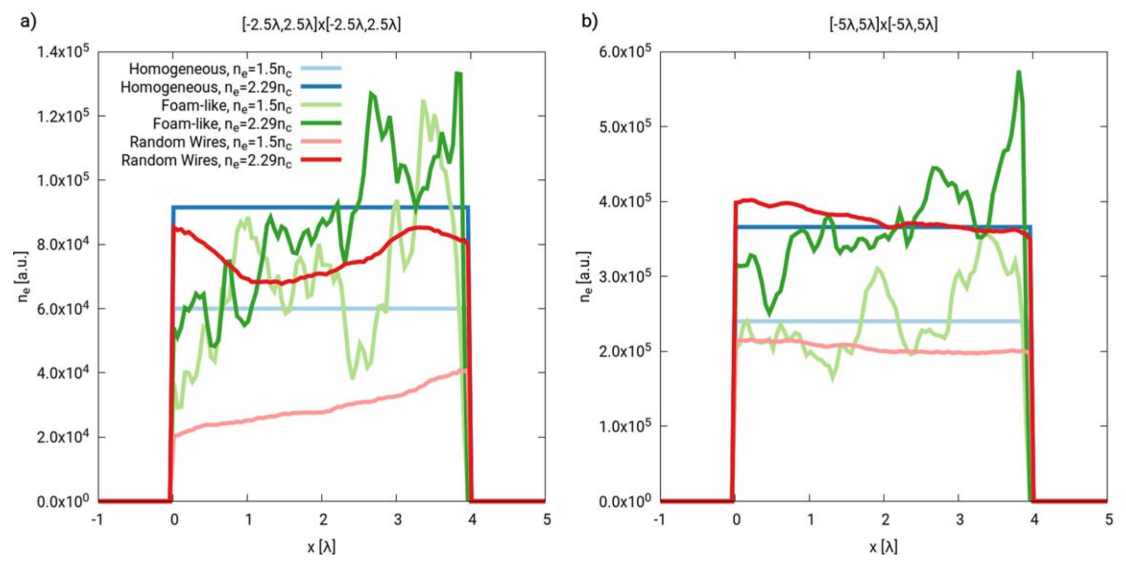

Figure 3. Integrated electron density profile as a function of the depth of the near-critical layer x, which is also the laser propagation direction (the laser hits the target at $x = 0$). The integration is performed over the transverse regions (a) $[-2.5\lambda, 2.5\lambda] \times [-2.5\lambda, 2.5\lambda]$ and (b) $[-5\lambda, 5\lambda] \times [-5\lambda, 5\lambda]$.

panel (b)), the fluctuations in the random wires are negligible, while those in the foams can be significant (up to a factor of 2).

2.2. MC simulations

We simulated the process of proton-to-neutron conversion via MC simulations. To this purpose, we employed the Geant4 (Geometry and Tracking) toolkit [67], which is widely used to simulate particle transport through matter in a variety of scenarios. Here, we are interested in a reliable description of neutron generation from nuclear reactions induced by moderate energy protons (~few MeVs). The main physical processes, i.e. the hadronic processes, were included via the `G4HadronPhysicsQGSP_BIC_AllHP` physics list, which was found to be the most reliable in a previous benchmarking work [68]. Due to the hadronic nature of the process, the primary bunch is only made of protons, whereas we disregarded electrons and photons coming from the prior laser-plasma interaction process. The proton momentum distribution is obtained from the 3D PIC simulations results. Indeed, 3D PIC simulations allow one to retrieve the full momentum distribution of any species. Therefore, we sampled the accelerated protons momentum distribution from the PIC output with the Inverse Transform Sampling method. Such sampling procedure is used in the MC code to initialize the energy and propagation direction of the primary proton bunch. The proton source is spatially point-like and is positioned 1.5 cm away from the converter. In each case, 10^{10} protons were shot. The converter is made of pure ^{9}beryllium with thickness equal to the range of the most energetic protons (0.009–0.06 cm). The main nuclear reactions at play are (p, n*).

3. Results

In this section we present the results of our numerical investigation, with a particular focus on ion acceleration and neutron generation. A brief discussion of the physical processes at play in ultra-intense laser-plasma interaction is provided as well.

3.1. Laser absorption into hot electrons

Laser absorption into electron kinetic energy in a near-critical plasma is a complicated, multifaceted process [52–54, 77]. In the case of a nanostructued plasma, the absorption process is further complicated by the inhomogeneities of the density profile, which are likely to be maintained during the interaction, especially because the ion dynamics is slower than the tens-of-fs laser temporal duration [65, 66]. In our scenario, the foam targets lead to an increased laser absorption into electrons. The flat target allows for ~10% conversion of laser energy into electron kinetic energy, while the remaining portion of the laser is mostly reflected. On the other hand, the DLTs allow for a maximum electron absorption of ~40%–60% (except for the denser homogeneous foam, which is too opaque for the considered pulse, for which it is ~20%). Depending on the morphology of the nanostructure, the absorption process leads to different features of the hot electron population, as shown in

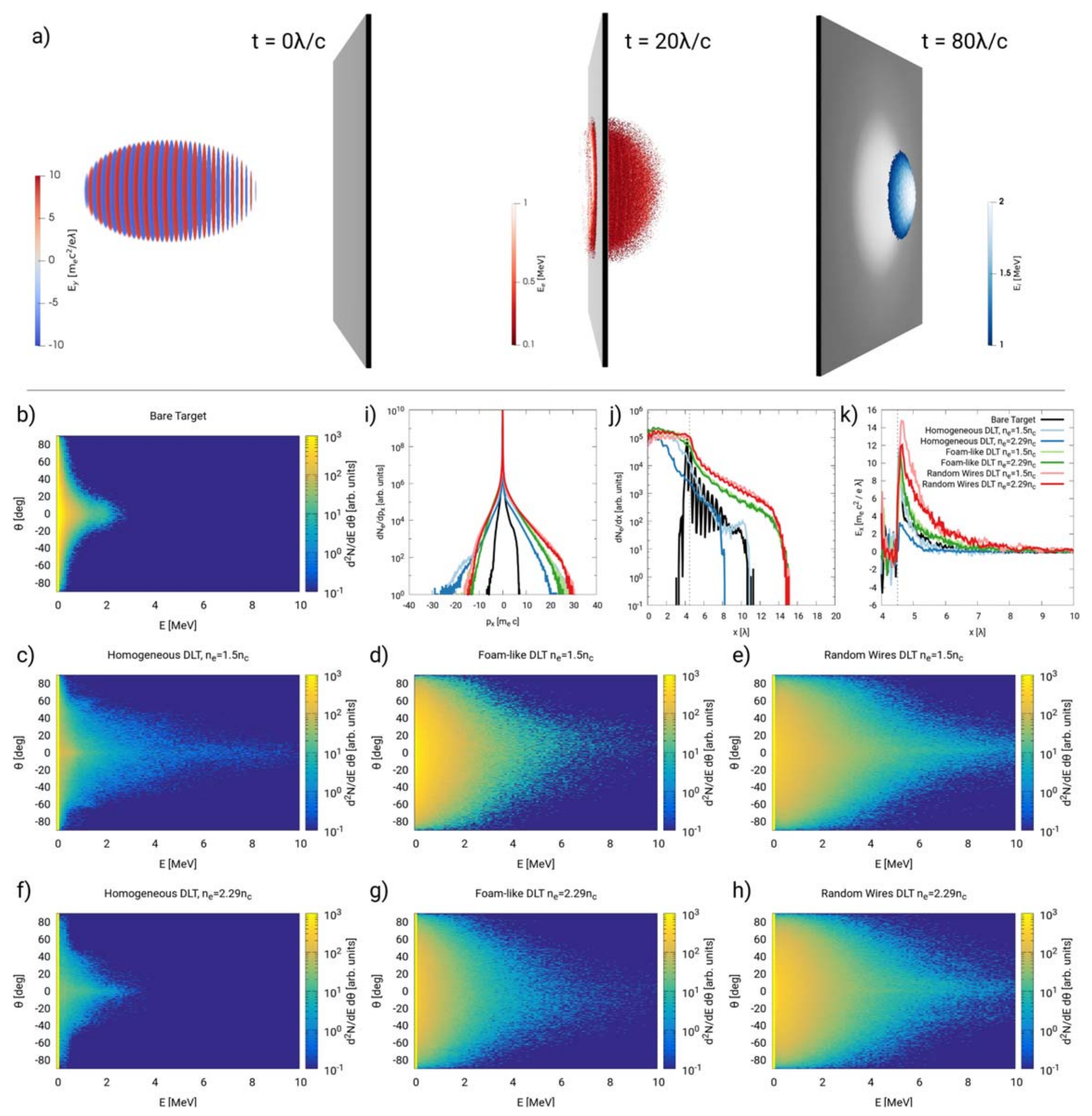

Figure 4. (a) Sketch of the TNSA process obtained with 3D PIC simulations at three time steps: at $t = 0\lambda/c$ the laser propagates towards the target, at $t = 20\lambda/c$ a population of relativistic electrons can be identified (red dots), at $t = 80\lambda/c$ the ions from the contaminant layer have been accelerated (blue dots). (b)–(h) The graphs show the projection of the hot electron phase space onto an energy-angle plane (the energy is measured in MeV and the angle is calculated with respect to target normal). (i) Momentum spectra ($\mathrm{d}N/\mathrm{d}p_x$) of the electron population for different targets. (j) Electron density ($\mathrm{d}N/\mathrm{d}x$) at the back side of the targets. (k) Longitudinal component of the electric field at the back side of the targets. The vertical dashed line in panels (i) and (j) represents the rear target surface. All the graphs are referred to time $t = 20\ \lambda/c$ and report results for the various target configurations described in this work.

figure 4. In particular, the presence of a near-critical nanostructured layer leads to significantly higher electron energies and a broader angular distribution. Concerning the homogeneous foams instead, the relatively dense $2.29\ n_c$ uniform layer is barely transparent for a $a_0 = 4$ laser beam. This means that the absorption efficiency is not significantly higher than for the flat target. The uniform foam with a density of $1.5n_c$ and the generation of hot electrons is improved, but still significantly below what is obtained with the nanostructured foams. These differences translate into different strengths and extensions of the quasi-static electrostatic fields at the back side of the target. Since the ion acceleration process is TNSA-like, these features have a profound influence on the properties of the accelerated ions. However, a detailed study of the absorption process requires an extensive, dedicated, investigation, which is not the focus of this manuscript and has been partially addressed elsewhere [55, 65, 66].

3.2. Enhanced laser-driven ion acceleration

Figure 5 shows the salient features of the accelerated ions obtained with the $2.29\ n_c$ foam-coated targets. The results for a simple flat target are reported as well for comparison. With respect to a simple flat target, the presence of the homogeneous foam leads only to a moderate enhancement of the cut-off energy of the accelerated ions (from ~2 to $\lesssim$3 MeV). On the contrary, the target coated with a fractal-like DLCCA foam

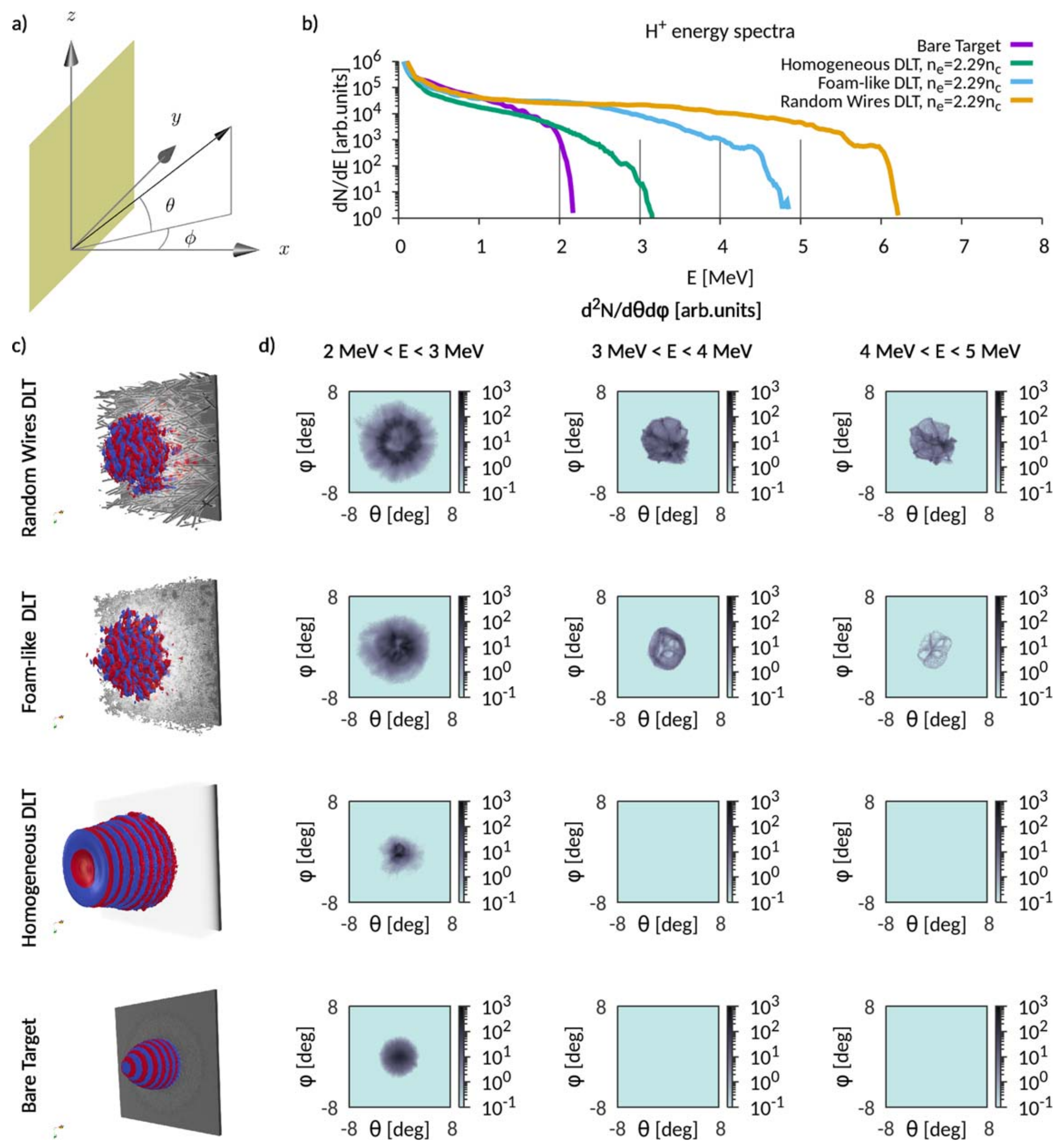

Figure 5. (a) Scheme to clarify the conventions used for the angles in the other panels. (b) Ion energy spectra for the three cases having $n_e = 2.29 n_c$ and for the monolayer target for comparison at time $80\lambda/c$. (c) Snapshots of the 3D PIC simulations at time $20\lambda/c$. The $\hat{z}$ component of the magnetic field is shown in blue-red scale, while the electron density is shown in grayscale. (d) 'Synthetic radiochromic films' at time $80\lambda/c$. Each panel shows the angular distribution of the emitted ions for a given energy range (indicated above) and for a given target configuration.

attains ∼4.5 MeV and the target coated with a random nanowire forest allows to obtain slightly more than 6 MeV, a 3× increase with respect to the simple flat target. These results are in agreement with what was observed for the electron population, since in a TNSA-like scheme a higher efficiency of laser-to-electrons coupling generally results into higher cut-off energies of the accelerated ions.

Concerning the angular distribution of the accelerated ions, the presence of a nanostructured layer seems to lead to a broader angular spread. Again, this is in agreement with what was observed for the electron population. Moreover, the angular distribution is much less homogeneous, with 'holes' and denser stripes appearing in the 'synthetic radiochromic film' diagnostic. These features are essentially irrelevant for the application of laser-driven proton sources considered here (neutron generation). However, they might be a severe hindrance if such a source is used for proton radiography, where having a smooth angular distribution is essential.

Figure 6 reports also the proton energy spectra obtained with foams having a lower average density (1.5 n_c). The most significant difference concerns the homogeneous foam: the lower density leads to a much greater laser absorption and therefore a higher maximum energy of the ions. For the structured foams, the lower average density has only a mild effect, slightly beneficial for the DLCCA foam and slightly disadvantageous for the nanowires foam. From the point of view of applications requiring stable ion fluxes, this mild dependence on the

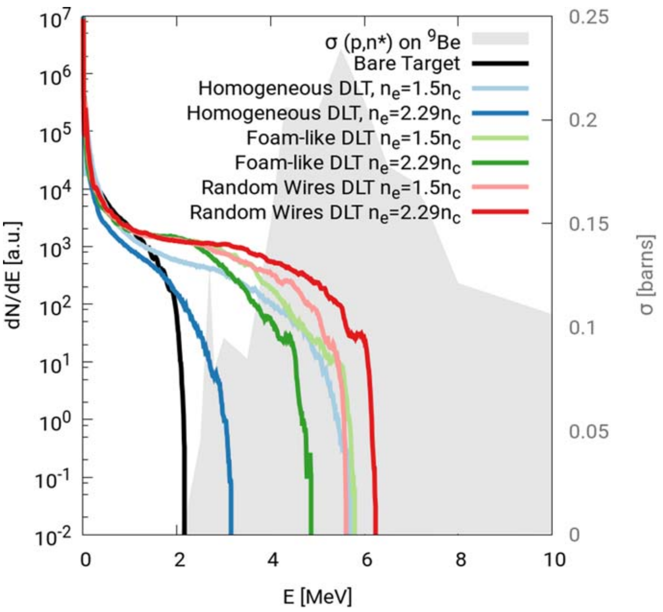

Figure 6. The graph shows the cross section for (p, n*) reaction in ^{9}Be (gray curve, right axis), together with the energy spectra of the accelerated ions for the different simulated scenarios obtained at $80\lambda/c$ (colored curves, left axis).

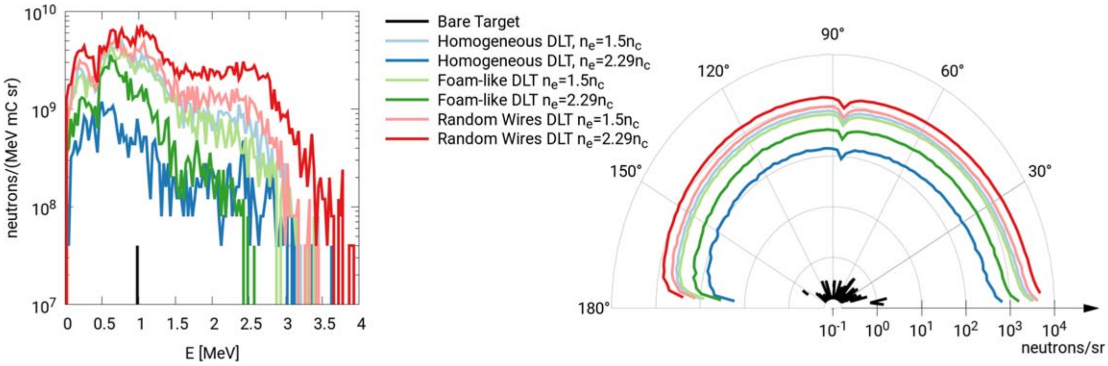

Figure 7. The panel on the left shows the energy distribution of the generated neutrons in all the simulated cases. The emission is integrated in a 15° cone around target normal in forward direction. The panel on the right shows the angular distribution of the emitted neutrons for all the simulated cases. 0° corresponds to the forward direction. The dent at ~90° corresponds neutrons propagating inside of the beryllium converter.

density could be a considerable advantage. The average density of nanostructured targets might change from sample to sample, due to unavoidable fluctuations in the manufacturing process. Our results suggest that the properties of an ion source based on these targets would remain relatively stable, even with large shot-to-shot variations of the target properties. This is further supported by results obtained in a previous work [66], where we considered laser interaction with nanostructured foams having quite different morphologies but the same average density, observing only a mild effect on laser absorption.

3.3. Enhanced neutron generation

Figure 6 represents the cross sections for the (p, n*) reaction in ^{9}Be, together with the energy spectra of the accelerated ions for all the simulated cases. Figure 7 illustrates the properties of the emitted neutrons in all the simulated cases, while figure 8 summarizes the proton-to-neutron conversion rate (top) and the total neutron yield (bottom). A first crucial observation is that accelerating protons at least up to 2 MeV is absolutely necessary to obtain neutron conversion, since this is the threshold for the nuclear reaction to take place. When the simple flat target is used for ion acceleration, the energy cut-off is barely above the 2 MeV threshold for neutron conversion (see figure 6), with extremely few ions having enough energy to have a non-zero chance of generating a neutron. This leads to a very low p-to-n conversion rate ($\sim 10^{-8}$ neutrons/protons), hence low neutron yield ($\sim 10^2$ neutrons/shot), as shown in figures 7 and 8. The presence of a near-critical layer leads to more ions having

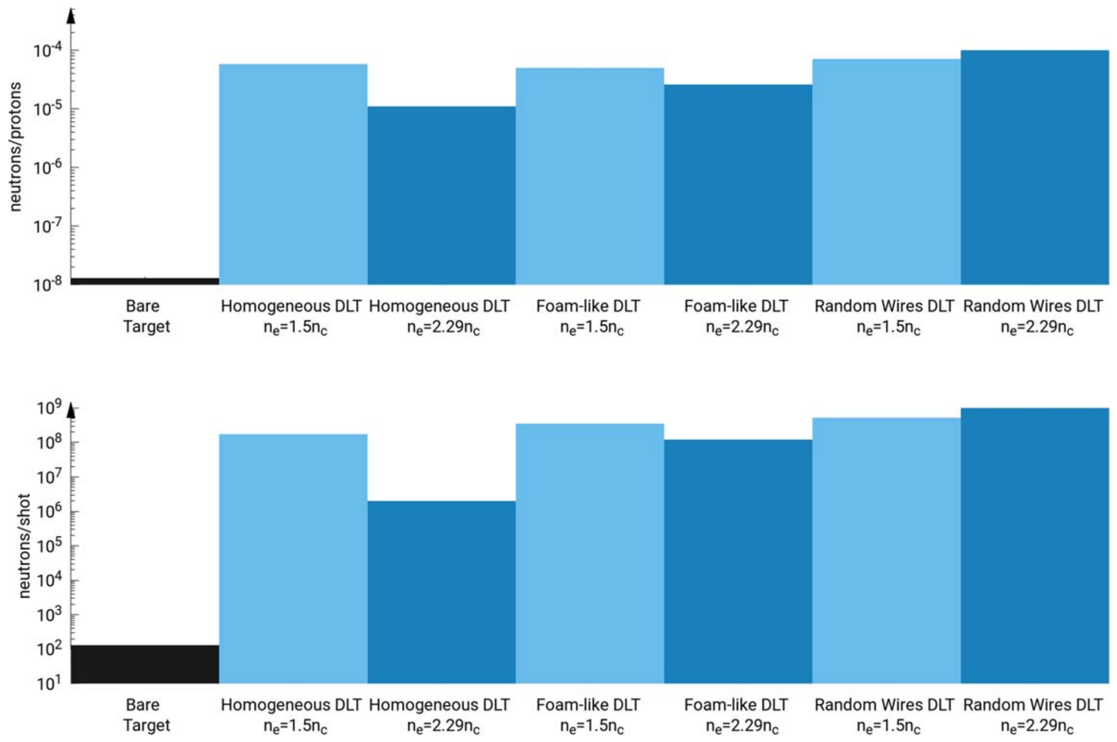

Figure 8. Top panel: conversion rate of protons into neutrons for all the simulated cases. Bottom panel: total neutron yield for all the simulated cases. Here, it is assumed that 10^{10} protons are accelerated to energies above 2 MeV with the bare target; the neutron yields obtained with the DLTs are scaled according to combined PIC and MC simulations results.

enough energy for a (p, n*) reaction (see figure 6). This leads to a very strong enhancement of the p-to-n conversion rate. Assuming that 10^{10} protons are accelerated above 2 MeV with the flat foil and taking into account the relative number of protons accelerated to energies above the reaction threshold, we also obtain a very strong enhancement (from 4 to 7 orders of magnitude) of the neutron yield with respect to the simple flat target, as shown in figure 8. Among the DLTs, the denser homogeneous foam is the worst performing case ($\sim 10^6$ neutrons/shot), while all the other cases fall within the 10^8–10^9 neutrons/shot range.

It is also worth highlighting that the cross section for (p, n*) reaction in ^{9}Be peaks at ~6 MeV (see figure 6, gray curve). Therefore, the proton energies obtained with the nanostructured targets are already enough to obtain optimal neutron conversion.

The left panel of figure 7 shows the energy spectra of the neutrons emitted in a 15° cone around the target normal in the forward direction. The distributions are quite broad, with a peak at 1–2 MeV and a cut-off extending up to 4 MeV, which means that the neutron source described here generates fast neutrons. A cut-off of ~4 MeV is coherent with a maximum ion energy of ~6 MeV and a negative *Q*-value of the (p, n*) reaction of ~ -1.85 MeV. Neutrons are emitted in all directions, as shown in the right panel of figure 7. However, the angular distribution is not uniform: about one order of magnitude more neutrons are emitted in forward direction. This could be beneficial for applications, also possibly mitigating radio-protection concerns.

4. Discussion

We presented a scheme of an ion source able to accelerate protons to an energy of few MeVs, driven by a moderately intense laser thanks to the use of nanostructured DLTs. We addressed the issue of setting up a description that takes into account non-trivial features, such as the details of the target nanostructure, the effect of a density fluctuation and the direct coupling with a p-to-n converter. Including these features in the description should be crucial if one expects some kind of quantitative agreement with experiments or aims at designing an actual source.

As discussed in the introduction, the few MeVs energy range is suitable for several applications in materials science. There exists a subset of applications requiring only a modest particle flux, such as the so-called proton induced x-ray emission spectroscopy [35], an ion beam analysis technique. This technique could be an ideal application of laser-driven ion sources [17], since few 10s of laser shots could be enough to complete a measurement. Our work represents a step forward in making the aforementioned moderate-energy applications of laser-driven ions a reality.

Adding a beryllium converter, we estimate that the laser-driven neutron source described in this work could provide $\sim 5 \times 10^5$ neutrons per laser shot if 10^{10} protons are accelerated to energies above the reaction threshold. Adopting targetry solutions analogous to those described in [70, 78] should allow operation of such a neutron source in a repetitive regime, for at least $\sim 10^3$ laser shots. Since compact 50 TW laser systems able to attain a repetition rate of ∼10 Hz are commercially available [79], we estimate a neutron flux of $\sim 5 \times 10^6$ n s^{-1} sustained for $\sim 10^2$ s to be within reach of existing technology. This seems doable from the practical point of view. In the most common configuration the target consists of a perforated holder upholding the DLT. In this case, the main limitation comes from the target transverse size and consequently from the number of holes that can be drilled in the holder. No actual limitation comes from having to grow the foam layer on a large substrate (in the worst case different targets may be juxtaposed). In previous experiments holders with ∼200 holes were employed, so that shooting hundreds of times at 1 Hz repetition rate seems doable. After that, a new target needs to be installed.

Our estimation for the neutron flux suggests that it could be comparable with that of other proposed compact laser-driven neutron sources reported in the literature, where for 'compact' we mean relying on table-top Ti:sapphire lasers not exceeding ∼100 TW. For instance, the interaction of a few mJ laser at kHz frequency with a heavy-water jet [80, 81] has been reported to lead to an average neutron yield of 2×10^5, while 2×10^6 neutrons per shot have been obtained via photoneutron generation with wakefield-accelerated electrons driven by a 0.5 J, 10 TW laser at $\sim 10^{-2}$ Hz [82]. Concerning schemes similar to that proposed here, where a target for ion acceleration and a separate converter for neutron generation are used, a yield of $\sim 10^6$ neutrons per steradian per shot can be obtained with few J lasers, but relying on deuterated targets (see [29] and references therein). In any case, it is worth remarking that the estimation of the yield of our source depends on our specific choices for the parameters of the contaminant layer, which are unfortunately not well characterized from the experimental point of view.

Conventional, portable, neutron sources based on deuterium-deuterium or deuterium–tritium fusion reaction can attain neutron fluxes two orders of magnitude higher than the source described here [83]. An improvement of the neutron yield for our source could be obtained using deuterated targets for ion acceleration, a strategy explored in several works [25–28, 32, 34]. Indeed, the ^{9}Be(d, n*) cross section is significantly higher than ^{9}Be(p, n*) cross section and the energy threshold for the projectile is lower [84]. This could allow to partially close the gap. However, the main strength of laser-driven neutron sources is not the average flux, for which competing with conventional sources seems to be a daunting task. Rather, the main advantages of a laser-driven sources lie in their pulsed nature and in their extremely short duration. A pulsed source could be beneficial to reduce signal-to-noise ratio in several applications (e.g. radiography or spectroscopy), since temporally gated detectors could be synchronized with the laser pulse. Indeed, 'flash neutron radiography' has been suggested in previous works as an application especially suited for laser-driven neutron sources [85]. Overall, our modeling approach could be used to guide the design and the optimization of these kinds of applications.

5. Conclusion

We have performed a numerical simulation campaign of a laser-driven ion acceleration scheme based on an advanced targetry solution, and of a neutron source based on this scheme.

DLTs consisting in a near-critical layer coupled to a solid foil can enhance the efficiency of the ion acceleration process, leading to more ions being accelerated up to higher energies. This results in a strong enhancement of the neutron yield when these ion sources are coupled with a suitable converter. Since one promising way to realize a near-critical layer consists in exploiting low-density nanostructured materials, we assessed the role of different realistic nanostructure morphologies on the ion acceleration process. We found that a realistic modeling of the nanostuctured target is essential to provide reliable indications for the design of experiments and for the development of laser-driven ion sources.

Our results suggest that nanostructured DLTs could be a crucial component to enable applications of hadron sources driven by compact, table-top lasers and our work provides essential tools for the numerical modeling of these schemes.

Acknowledgments

We thank Francesco Mirani, Politecnico di Milano (Italy), for useful discussions and for his assistance on the set-up of the Monte Carlo simulations. This project has received funding from the European Research Council (ERC) under the European Union's Horizon 2020 research and innovation programme (ENSURE grant agreement No 647 554 and INTER grant agreement No 754 916). We also acknowledge Iscra access scheme to MARCONI and GALILEO High Performance Computing machine at CINECA (Casalecchio di Reno, Bologna, Italy) via the projects IRONMAN, PIMIENTO and ELF.

ORCID iDs

L Fedeli https://orcid.org/0000-0002-7215-4178
M Passoni https://orcid.org/0000-0002-7844-3691

References

[1] Daido H, Nishiuchi M and Pirozhkov A S 2012 Review of laser-driven ion sources and their applications *Rep. Prog. Phys.* **75** 056401
[2] Macchi A, Borghesi M and Passoni M 2013 Ion acceleration by superintense laser-plasma interaction *Rev. Mod. Phys.* **85** 751–93
[3] Schreiber J, Bolton P R and Parodi K 2016 Invited review article: 'hands-on' laser-driven ion acceleration: a primer for laser-driven source development and potential applications *Rev. Sci. Instrum.* **87** 071101
[4] Jong Kim I *et al* 2016 Radiation pressure acceleration of protons to 93 MeV with circularly polarized petawatt laser pulses *Phys. Plasmas* **23** 070701
[5] Wagner F *et al* 2016 Maximum proton energy above 85 MeV from the relativistic interaction of laser pulses with micrometer thick CH_2 targets *Phys. Rev. Lett.* **116** 205002
[6] Higginson A *et al* 2018 Near-100 MeV protons via a laser-driven transparency-enhanced hybrid acceleration scheme *Nat. Commun.* **9** 724
[7] Wilks S C, Langdon A B, Cowan T E, Roth M, Singh M, Hatchett S, Key M H, Pennington D, MacKinnon A and Snavely R A 2001 Energetic proton generation in ultra-intense laser-solid interactions *Phys. Plasmas* **8** 542–9
[8] Bulanov S V and Khoroshkov V S 2002 Feasibility of using laser ion accelerators in proton therapy *Plasma Phys. Rep.* **28** 453–6
[9] Linz U and Alonso J 2007 What will it take for laser driven proton accelerators to be applied to tumor therapy? *Phys. Rev. ST Accel. Beams* **10** 094801
[10] Linz U and Alonso J 2016 Laser-driven ion accelerators for tumor therapy revisited *Phys. Rev. Accel. Beams* **19** 124802
[11] Borghesi M *et al* 2002 Electric field detection in laser-plasma interaction experiments via the proton imaging technique *Phys. Plasmas* **9** 2214–20
[12] Mackinnon A J *et al* 2006 Proton radiography of a laser-driven implosion *Phys. Rev. Lett.* **97** 045001
[13] Borghesi M *et al* 2008 Laser-driven proton acceleration: source optimization and radiographic applications *Plasma Phys. Control. Fusion* **50** 124040
[14] Barberio M, Veltri S, Scisciò M and Antici P 2017 Laser-accelerated proton beams as diagnostics for cultural heritage *Sci. Rep.* **7** 40415
[15] Mirani F 2017 Ion beam analysis with laser-driven proton beams *Master's Thesis* Politecnico di Milano, Italy http://hdl.handle.net/10589/135905
[16] Barberio M and Antici P 2019 Laser-PIXE using laser-accelerated proton beams *Sci. Rep.* **9** 6855
[17] Passoni M, Fedeli L and Mirani F 2019 Superintense laser-driven ion beam analysis *Sci. Rep.* **9** 9202
[18] Hidding B *et al* 2017 Laser-plasma-based space radiation reproduction in the laboratory *Sci. Rep.* **7** 42354
[19] Barberio M *et al* 2018 Laser-accelerated particle beams for stress testing of materials *Nat. Commun.* **9** 372
[20] Dromey B *et al* 2016 Picosecond metrology of laser-driven proton bursts *Nat. Commun.* **7** 10642
[21] Taylor M *et al* 2018 Probing ultrafast proton induced dynamics in transparent dielectrics *Plasma Phys. Control. Fusion* **60** 054004
[22] Barberio M and Antici P 2017 Laser-plasma driven synthesis of carbon-based nanomaterials *Sci. Rep.* **7** 12009
[23] Barberio M, Scisciò M, Vallières S, Veltri S, Morabito A and Antici P 2017 Laser-generated proton beams for high-precision ultra-fast crystal synthesis *Sci. Rep.* **7** 12522
[24] Lancaster K L *et al* 2004 Characterization of 7Li(p, n)7Be neutron yields from laser produced ion beams for fast neutron radiography *Phys. Plasmas* **11** 3404–8
[25] Petrov G M, Higginson D P, Davis J, Petrova Tz B, McNaney J M, McGuffey C, Qiao B and Beg F N 2012 Generation of high-energy (>15 MeV) neutrons using short pulse high intensity lasers *Phys. Plasmas* **19** 093106
[26] Maksimchuk A, Raymond A, Yu F, Petrov G M, Dollar F, Willingale L, Zulick C, Davis J and Krushelnick K 2013 Dominant deuteron acceleration with a high-intensity laser for isotope production and neutron generation *Appl. Phys. Lett.* **102** 191117
[27] Zulick C *et al* 2013 Energetic neutron beams generated from femtosecond laser plasma interactions *Appl. Phys. Lett.* **102** 124101
[28] Kar S *et al* 2016 Beamed neutron emission driven by laser accelerated light ions *New J. Phys.* **18** 053002
[29] Alejo A, Borghesi M, Kar S, Ahmed H, Green A and Mirfayzi S R 2016 Recent advances in laser-driven neutron sources *Nuovo Cim.* **38** 188
[30] Mirfayzi S R *et al* 2017 Experimental demonstration of a compact epithermal neutron source based on a high power laser *Appl. Phys. Lett.* **111** 044101
[31] Brenner C M *et al* 2016 Laser-driven x-ray and neutron source development for industrial applications of plasma accelerators *Plasma Phys. Control. Fusion* **58** 014039
[32] Favalli A *et al* 2019 Characterizing laser-plasma ion accelerators driving an intense neutron beam via nuclear signatures *Sci. Rep.* **9** 2004
[33] Higginson D P *et al* 2010 Laser generated neutron source for neutron resonance spectroscopy *Phys. Plasmas* **17** 100701
[34] Roth M *et al* 2013 Bright laser-driven neutron source based on the relativistic transparency of solids *Phys. Rev. Lett.* **110** 044802
[35] Verma H R 2007 *Atomic and Nuclear Analytical Methods: XRF, Mössbauer, XPS, NAA and Ion-Beam Spectroscopic Techniques* (Berlin: Springer) (https://doi.org/10.1007/978-3-540-30279-7)
[36] Macklin R L and Gibbons J H 1958 Study of the $T(p, n)He^3$ and $Li^7(p, n)Be^7$ reactions *Phys. Rev.* **109** 105–9
[37] Marion J B 1956 Excited states in B^{10} *Phys. Rev.* **103** 713–7
[38] Morrison J T *et al* 2018 Mev proton acceleration at kHz repetition rate from ultra-intense laser liquid interaction *New J. Phys.* **20** 022001
[39] Borghesi M and Schramm U 2016 Summary of working group 2: ion beams from plasmas *2nd European Advanced Accelerator Concepts Workshop-EAAC 2015; Nucl. Instrum. Methods Phys. Res.* A **829** 137–40
[40] Flacco A and Willingale L 2018 Summary of working group 2: ion beams from plasmas *3rd European Advanced Accelerator Concepts Workshop (EAAC2017); Nucl. Instrum. Methods Phys. Res.* A **909** 153–5

[41] Zani A, Dellasega D, Russo V and Passoni M 2013 Ultra-low density carbon foams produced by pulsed laser deposition *Carbon* **56** 358–65
[42] Nagai K, Musgrave C S A and Nazarov W 2018 A review of low density porous materials used in laser plasma experiments *Phys. Plasmas* **25** 030501
[43] Yogo A *et al* 2008 Laser ion acceleration via control of the near-critical density target *Phys. Rev.* E **77** 016401
[44] Willingale L *et al* 2009 Characterization of high-intensity laser propagation in the relativistic transparent regime through measurements of energetic proton beams *Phys. Rev. Lett.* **102** 125002
[45] Nakamura T, Tampo M, Kodama R, Bulanov S V and Kando M 2010 Interaction of high contrast laser pulse with foam-attached target *Phys. Plasmas* **17** 113107
[46] Sgattoni A, Londrillo P, Macchi A and Passoni M 2012 Laser ion acceleration using a solid target coupled with a low-density layer *Phys. Rev.* E **85** 036405
[47] Passoni M *et al* 2014 Energetic ions at moderate laser intensities using foam-based multi-layered targets *Plasma Phys. Control. Fusion* **56** 045001
[48] Prencipe I *et al* 2016 Development of foam-based layered targets for laser-driven ion beam production *Plasma Phys. Control. Fusion* **58** 034019
[49] Passoni M *et al* 2016 Toward high-energy laser-driven ion beams: nanostructured double-layer targets. *Phys. Rev. Accel. Beams* **19** 061301
[50] Bin J H *et al* 2018 Enhanced laser-driven ion acceleration by superponderomotive electrons generated from near-critical-density plasma *Phys. Rev. Lett.* **120** 074801
[51] Ma W J *et al* 2019 Laser acceleration of highly energetic carbon ions using a double-layer target composed of slightly underdense plasma and ultrathin foil *Phys. Rev. Lett.* **122** 014803
[52] Pukhov A and Meyer-ter Vehn J 1996 Relativistic magnetic self-channeling of light in near-critical plasma: three-dimensional particle-in-cell simulation *Phys. Rev. Lett.* **76** 3975
[53] Borghesi M, MacKinnon A J, Barringer L, Gaillard R, Gizzi L A, Meyer C, Willi O, Pukhov A and Meyer-ter Vehn J 1997 Relativistic channeling of a picosecond laser pulse in a near-critical preformed plasma *Phys. Rev. Lett.* **78** 879
[54] Robinson A P L, Trines R M G M, Polz J and Kaluza M 2011 Absorption of circularly polarized laser pulses in near-critical plasmas *Plasma Phys. Control. Fusion* **53** 065019
[55] Cialfi L, Fedeli L and Passoni M 2016 Electron heating in subpicosecond laser interaction with overdense and near-critical plasmas *Phys. Rev.* E **94** 053201
[56] Fedeli L, Formenti A, Cialfi L, Sgattoni A, Cantono G and Passoni M 2018 Structured targets for advanced laser-driven sources *Plasma Phys. Control. Fusion* **60** 014013
[57] Batani D *et al* 2010 Effects of laser prepulses on laser-induced proton generation *New J. Phys.* **12** 045018
[58] Kaluza M, Schreiber J, Santala M IK, Tsakiris G D, Eidmann K, Meyer-ter Vehn J and Witte K J 2004 Influence of the laser prepulse on proton acceleration in thin-foil experiments *Phys. Rev. Lett.* **93** 045003
[59] Flacco A, Sylla F, Veltcheva M, Carrié M, Nuter R, Lefebvre E, Batani D and Malka V 2010 Dependence on pulse duration and foil thickness in high-contrast-laser proton acceleration *Phys. Rev.* E **81** 036405
[60] Gray R J *et al* 2014 Laser pulse propagation and enhanced energy coupling to fast electrons in dense plasma gradients *New J. Phys.* **16** 113075
[61] Ceccotti T, Lévy A, Popescu H, Réau F, d'Oliveira P, Monot P, Geindre J P, Lefebvre E and Martin P 2007 Proton acceleration with high-intensity ultrahigh-contrast laser pulses *Phys. Rev. Lett.* **99** 185002
[62] Yu T J, Lee S K, Sung J H, Yoon J W, Jeong T M and Lee J 2012 Generation of high-contrast, 30 fs, 1.5 PW laser pulses from chirped-pulse amplification ti:sapphire laser *Opt. Express* **20** 10807–15
[63] Schramm U *et al* 2017 First results with the novel petawatt laser acceleration facility in dresden *8th Int. Particle Accelerator Conf. (IPAC'17) (Copenhagen, Denmark, 14â 19 May)* pp 48–52 JACOW, Geneva, Switzerland
[64] Obst L *et al* 2018 On-shot characterization of single plasma mirror temporal contrast improvement *Plasma Phys. Control. Fusion* **60** 054007
[65] Fedeli L, Formenti A, Bottani C E and Passoni M 2017 Parametric investigation of laser interaction with uniform and nanostructured near-critical plasmas. *Eur. Phys. J.* D **71** 202
[66] Fedeli L, Formenti A, Cialfi L, Pazzaglia A and Passoni M 2018 Ultra-intense laser interaction with nanostructured near-critical plasmas *Sci. Rep.* **8** 3834
[67] Agostinelli S *et al* 2003 Geant4—a simulation toolkit *Nucl. Instrum. Methods Phys. Res.* A **506** 250–303
[68] Tentori A 2018 Laser-driven neutron sources: a first numerical investigation *Master's Thesis* Politecnico di Milano, Italy http://hdl.handle.net/10589/139122
[69] Arioli F M 2018 Compact laser-driven neutron sources: a theoretical investigation *Master's Thesis* Politecnico di Milano, Italy http://hdl.handle.net/10589/142386
[70] Prencipe I *et al* 2017 Targets for high repetition rate laser facilities: needs, challenges and perspectives *High Power Laser Sci. Eng.* **5** e17
[71] Birdsall C K and Langdon A B 1985 *Plasma Physics Via Computer Simulation* (New York: Mc Graw-Hill) (https://doi.org/10.1201/9781315275048)
[72] Arber T D *et al* 2015 Contemporary particle-in-cell approach to laser-plasma modelling *Plasma Phys. Control. Fusion* **57** 113001
[73] Sgattoni A *et al* 2015 *Optimising PICCANTE—an open source particle-in-cell code for advanced simulations on Tier-0 systems* arXiv:1503.02464
[74] Bargsten C *et al* 2017 Energy penetration into arrays of aligned nanowires irradiated with relativistic intensities: scaling to Terabar pressures *Sci. Adv.* **3** e1601558
[75] Cristoforetti G *et al* 2017 Transition from coherent to stochastic electron heating in ultrashort relativistic laser interaction with structured targets *Sci. Rep.* **7** 1479
[76] Meakin P 1983 Formation of fractal clusters and networks by irreversible diffusion-limited aggregation *Phys. Rev. Lett.* **51** 1119–22
[77] Askar'Yan G A, Bulanov S V, Pegoraro F and Pukhov A M 1994 Magnetic interaction of self-focusing channels and fluxes of electromagnetic radiation: their coalescence, the accumulation of energy, and the effect of external magnetic fields on them *JETP Lett.* **60** 251–7
[78] Zaffino R L *et al* 2018 Wafer-scale fabrication of target arrays for stable generation of proton beams by laser-plasma interaction *J. Phys.: Conf. Ser.* **1079** 012007
[79] Thales, Paris, France. *QUARK 45: Ultrafast Ti:Sa Laser Series, https://perma.cc/U9EP-W9X5* (accessed: 20-September-2019)

[80] Hah J, Petrov G M, Nees J A, He Z-H, Hammig M D, Krushelnick K and Thomas A G R 2016 High repetition-rate neutron generation by several-mJ, 35 fs pulses interacting with free-flowing d2o *Appl. Phys. Lett.* **109** 144102

[81] Hah J, Nees J A, Hammig M D, Krushelnick K and Thomas A G R 2018 Characterization of a high repetition-rate laser-driven short-pulsed neutron source *Plasma Phys. Control. Fusion* **60** 054011

[82] Jiao X J *et al* 2017 A tabletop, ultrashort pulse photoneutron source driven by electrons from laser wakefield acceleration *Matter Radiat. Extremes* **2** 296–302

[83] Chichester D L, Simpson J D and Lemchak M 2007 Advanced compact accelerator neutron generator technology for active neutron interrogation field work *J. Radioanal. Nucl. Chem.* **271** 629–37

[84] Koning A J and Rochman D 2012 Modern nuclear data evaluation with the TALYS code system *Nucl. Data Sheets* **113** 2841–934 Special Issue on Nuclear Reaction Data

[85] Guler N *et al* 2016 Neutron imaging with the short-pulse laser driven neutron source at the Trident laser facility *J. Appl. Phys.* **120** 154901